Alterations in Myocardial Cardiolipin Content and Composition Occur at the Very Earliest Stages of Diabetes: A Shotgun Lipidomics Study

Xianlin Han‡,§,*, **Jingyue Yang**‡, **Kui Yang**‡, **Zhongdan, Zhao**‡, **Dana R. Abendschein**§,‖, and **Richard W. Gross**‡,§,⊥,#

Division of Bioorganic Chemistry and Molecular Pharmacology, Division of Cardiology, Department of Internal Medicine, and Department of Molecular Biology and Pharmacology, Washington University School of Medicine, St. Louis, Missouri 63110, and Department of Chemistry, Washington University, St. Louis, Missouri 63130

‡ *Division of Bioorganic Chemistry and Molecular Pharmacology, Washington University School of Medicine.*

§ *Department of Internal Medicine, Washington University School of Medicine.*

‖ *Division of Cardiology, Washington University School of Medicine.*

⊥ *Department of Molecular Biology and Pharmacology, Washington University School of Medicine.*

Department of Chemistry, Washington University.

Abstract

Recently, we have identified the dramatic depletion of cardiolipin (CL) in diabetic myocardium 6 weeks after streptozotocin (STZ) injection that was accompanied by increases in triacylglycerol content and multiple changes in polar lipid molecular species. However, after 6 weeks in the diabetic state, the predominant lipid hallmarks of diabetic cardiomyopathy were each present concomitantly, and thus, it was impossible to identify the temporal course of lipid alterations in diabetic myocardium. Using the newly developed enhanced shotgun lipidomics approach, we demonstrated the dramatic loss of abundant CL molecular species in STZ-treated hearts at the very earliest stages of diabetes accompanied by a profound remodeling of the remaining CL molecular species including a 16-fold increase in the content of 18:2−22:6−22:6−22:6 CL. These alterations in CL metabolism occur within days after the induction of the diabetic state and precede the triacylglycerol accumulation manifest in diabetic myocardium. Similarly, in *ob/ob* mice, a dramatic and progressive redistribution from 18:2 FA-containing CL molecular species to 22:6 FA-containing CL molecular species was also identified. Collectively, these results demonstrate alterations in CL hydrolysis and remodeling at the earliest stages of diabetes and are consistent with a role for alterations in CL content in precipitating mitochondrial dysfunction in diabetic cardiomyopathy.

Diabetic cardiomyopathy is characterized by the presence of marked alterations in the lipid composition of myocardium, inefficient substrate utilization, and diastolic dysfunction (1–9). Many studies have implicated mitochondrial dysfunction (1,2,4,5,7–11) as the underlying mechanism that precipitates hemodynamic dysfunction and contributes to the untoward sequelae of events in diabetic patients following myocardial ischemia. Persistent changes in substrate utilization occur in diabetic myocardium with an increased utilization of fatty acid

substrate and a decreased dependence on glucose. Increased fatty acid utilization promotes the generation of reactive oxygen species which can oxidize highly unsaturated lipids in the mitochondrial compartment such as cardiolipin (CL)[1] and impair mitochondrial function. Collectively, these features each contribute to the accumulation of toxic lipids in diabetic myocardium [e.g., acylcarnitines, acyl-CoAs, and triacylglycerols (TG)] that compromise the functional integrity of many membrane systems (2,4,5,7,9). In early studies, we and others identified profound alterations in the myocardial lipid composition in obese and diabetic rats, which were accompanied by physiologic dysfunction (1,2). The abnormalities in lipid metabolism present in diabetic myocardium include the accumulation of acylcarnitines, thereby directly implicating mitochondrial dysfunction as a likely contributing mechanism to the compromised metabolic and hemodynamic efficiency of diabetic myocardium. The recent appreciation of these processes has led to the widespread agreement that diabetic cardiomyopathy is a metabolic myopathy involving alterations in lipid metabolism and mitochondrial function, but the biochemical mechanisms responsible are not known with certainty.

CL is a class of atypical phospholipids that plays an essential role in mitochondrial bioenergetics and cellular apoptosis. In mammals, CL is localized predominantly in the mitochondrial inner membrane where it facilitates mitochondrial function through a variety of mechanisms largely related to its highly anionic character, large aliphatic chain to polar head group volume, and binding to specific proteins in the mitochondria such as those in the electron transport chain (e.g., cytochrome c oxidase) (12–15). The essential role of CL in mitochondrial function and cardiac hemodynamic function has recently been underscored by the identification of the genetic basis of Barth syndrome, in which mutations in an X-linked gene, tafazzin, induce alterations in CL metabolism, precipitate mitochondrial dysfunction, and result in a striking cardiomyopathy (16–23). Accordingly, the cause and effect relationship between alterations in CL metabolism and compromised mitochondrial and cardiac hemodynamic function are now well accepted. The pathological decrease in CL content and altered CL aliphatic chain composition in Barth syndrome have recently been shown to be initiated by the action of a mitochondrial phospholipase (leading to the formation of monolysoCL) followed by a nonselective acyl transfer reaction catalyzed by tafazzin mutants (24). Therefore, the molecular species of CL which is predominant under normal physiological conditions (i.e., tetra 18:2 CL or T18:2 CL) in almost all known mammalian mitochondrial membranes is altered in patients with Barth syndrome (25).

Previously, alterations in CL were difficult to measure due to intractable technical problems. However, through the development of shotgun lipidomics, which utilizes intrasource separation and multidimensional mass spectrometry (MS) (26–29), we have recently demonstrated the substantial depletion of the predominant CL molecular species present in myocardium (e.g., T18:2 CL) in mice rendered diabetic for 6 weeks by streptozotocin (STZ) treatment (6). Based upon prior studies from multiple independent laboratories, the magnitude of CL depletion and/or changes in CL molecular composition that we have demonstrated in diabetic myocardium would be predicted to result in severe defects in the function of the mitochondrial electron transport chain, facilitating free radical generation.

To identify the temporal course of alterations in CL content and molecular species composition induced by diabetes and their potential role in mediating the altered metabolism present in the diabetic state, we have recently developed a novel enhanced shotgun lipidomics approach for

---

[1]Abbreviations: CL, cardiolipin; ESI, electrospray ionization; FA, fatty acyl; FFA, nonesterified fatty acid; GPA, phosphatidic acid; GPCho, choline glycerophospholipids; GPEtn, ethanolamine glycerophospholipids; GPGro, phosphatidylglycerol(s); GPIns, phosphatidylinositol(s); GPSer, phosphatidylserine(s); $m{:}n$, acyl chain containing m carbons and n double bonds; MS, mass spectrometry; NL, neutral loss; SEM, standard error of the mean; SM, sphingomyelin; STZ, streptozotocin; TG, triacylglycerol; TIC, total ion current; T$m{:}n$ TG, tri-m: n-glycerol; WT, wild type.

the analysis of individual CL molecular species based on their specific chemical features (30). Herein, we used this approach to identify the rapid and dramatic loss of abundant CL molecular species (e.g., T18:2 CL and 18:1−18:2−18:2−18:2 CL) at the earliest stages of diabetes and to demonstrate the unanticipated accumulation of the docosahexaenoate- (22:6 FA-) containing CL molecular species in the diabetic state. Moreover, we also show that alterations in CL content and molecular species composition precede TG accumulation in STZ-induced diabetic myocardium or occur in parallel with TG accumulation in *ob*/*ob* mouse myocardium. Collectively, these results provide new insights into the temporal course of alterations in lipid metabolism during the induction of the diabetic state that likely underlie the pathogenesis of mitochondrial dysfunction in diabetic cardiomyopathy.

MATERIALS AND METHODS

Materials

Synthetic phospholipids including 1,1′,2,2′-tetramyristoylcardiolipin (T14:0 CL), 1,2-dimyristoleoyl-*sn*-glycero-3-phosphocholine (14:1−14:1 GPCho), 1,2-dipentadecanoyl-*sn*-glycero-3-phosphoethanolamine (15:0−15:0 GPEtn), 1,2-dipentadecanoyl-*sn*-glycero-3-phosphoglycerol (15:0−15:0 GPGro), 1,2-dimyristoyl-*sn*-glycero-3-phosphoserine (14:0−14:0 GPSer), 1,2-dimyristoyl-*sn*-glycerol 3-phosphate (14:0−14:0 GPA), 1-heptadecanoyl-2-hydroxy-*sn*glycero-3-phosphocholine (17:0 lysoGPCho), 1-myristoyl-2-hydroxy-*sn*-glycero-3-phosphoethanolamine(14:0lysoGPEtn), *N*-laurorylsphingomyelin (N12:0 SM), and *N*-heptadecanoylceramide (N17:0 Cer) were purchased from Avanti Polar Lipids, Inc. (Alabaster, AL). Deuterated palmitic acid (d_4−16:0 FA) was purchased from Cambridge Isotope Laboratories, Inc. (Cambridge, MA). Triheptadecanoylglycerol (T17:1 TG) was purchased from Nu Chek, Inc. (Elysian, MN). All of these lipids were quantitated by capillary gas chromatography after methanolysis (31). Heptadecanoyl-CoA (17:0 CoA) was purchased from Sigma-Aldrich Chemical Co. (St. Louis, MO). Solvents for sample preparation and for mass spectrometric analysis were obtained from Burdick and Jackson (Honeywell International Inc., Burdick and Jackson, Muskegon, MI). All other chemical reagents were of at least analytical grade or the best grade available and were obtained from either Fisher Scientific (Pittsburgh, PA) or Sigma-Aldrich Chemical Co. (St. Louis, MO) or as indicated.

Induction of Diabetes and Sample Preparation

Male wild-type mice (C57BL/6, 4 months of age) and *ob*/*ob* mice (C57BL/6, at the indicated ages) were purchased from The Jackson Laboratory (Bar Harbor, ME). Diabetes in 4-month-old wild-type mice was induced by a single intravenous injection (in the tail vein) of STZ (165 mg/kg body weight in 0.1 mL of 0.1 M citrate buffer, pH 4.5) as described previously (2). Control mice received citrate buffer (0.1 mL) alone. Diabetes was confirmed within 48 h by blood glucose levels >3 mg/mL as measured by chemstrips (bG; Boehringer-Mannheim). All animal procedures were performed in accordance with the Guide for the Care and Use of Laboratory Animals (National Academy of Sciences, 1996) and were approved by the Animals Studies Committee at Washington University.

Mice were killed by asphyxiation with carbon dioxide after diabetes was induced for the indicated time intervals or at the indicated ages for *ob*/*ob* mice. The hearts were excised quickly and immersed in ice-cooled 10-fold-diluted phosphate-buffered saline. After extraneous tissue and epicardial fat were removed, each heart was quickly dried and immediately freeze-clamped at the temperature of liquid nitrogen. Myocardial wafers were pulverized into a fine powder with a stainless steel mortar and pestle. Protein assays on the wafers were performed using a bicinchoninic acid protein assay kit (Pierce, Rockford, IL) with bovine serum albumin as a standard.

A myocardial sample (approximately 10 mg) was weighed from each mouse heart. Internal standards for global lipid analysis including 14:0−14:0 GPSer (4.0 nmol/mg of protein), 14:0 −14:0 GPA (0.75 nmol/mg of protein), N12:0 SM (2 nmol/mg of protein), T14:0 CL (4.0 nmol/mg of protein), 15:0−15:0 GPGro (2 nmol/mg of protein), 15:0−15:0 GPEtn (19 nmol/mg of protein), 14:1−14:1 GPCho (15 nmol/mg of protein), 17:0 lysoGPCho (1.5 nmol/mg of protein), 14:0 lysoGPEtn (1.5 nmol/mg of protein), T17:1 TG (7.5 nmol/mg of protein), N17:0 Cer (40 pmol/mg of protein), and d_4−16:0 FA (2 nmol/mg protein) were added to each myocardial sample on the basis of protein concentration prior to extraction of lipids. Thus, the lipid content can be normalized to the protein content and quantified directly. These internal standards were selected because they represent <<1% of endogenous cellular lipid molecular species present as demonstrated through molecular species profiling by electrospray ionization (ESI) MS without addition of these internal standards.

Lipids were extracted by the modified method of Bligh and Dyer (32) and filtered as described previously (6). Each individual myocardial lipid extract was reconstituted with a volume of 100 μL/mg protein (which was based on the original protein content of the samples as determined from protein assays) in 1:1 chloroform/methanol. The lipid extracts were finally flushed with nitrogen, capped, and stored at −20°C (typically analyzed within 1 week which is critical for CL analysis). Each lipid solution was further diluted approximately 200-fold just prior to infusion and lipid analysis. To the diluted lipid solutions, LiOH (50 nmol/mg of protein) was added immediately prior to performing further lipid analyses in both negative- and positive-ion modes when necessary (27). Sample preparation of lipid extracts for acyl-CoA analyses was performed in the presence of an internal standard [i.e., 17:0 CoA (30 pmol/mg of protein)] as previously described (33). Tandem MS analyses of acyl-CoA molecular species by using precursor-ion scanning were conducted as previously described (34).

Instrumentation and Mass Spectrometry

Shotgun lipidomics analyses of CL molecular species were performed on a QqTOF mass spectrometer (Applied Biosystems/MDS Sciex QStar XL, Concord, Canada) equipped with an ion spray ion source as previously described (30). Before sample analyses, the mass spectrometer was tuned and calibrated in the negative-ion mode using a mixture of T14:0 CL and T18:1 CL to optimize the resolution and mass accuracy. Typically, a resolution of ~11000 at m/z 727 was employed. Diluted lipid extract was infused into the mass spectrometer at a flow rate of 4 μL/min through a Harvard syringe pump. The mass spectrometer was operated in the negative-ion TOF-MS mode with the following parameter settings: spray voltage, −4.5 kV; declustering potential, −60 V; focusing potential, −265 V; declustering potential 2, −15 V; ion source gas, scale 2; curtain gas, scale 20; collision gas, 2 mTorr; ion release delay, 2 ms; mass/charge range, 600−1000 Th; Q1 ion transmission setting, 580/50% and 772/50% (27). The spray stability was monitored by total ion count to ensure less than 10% relative variation. Typically, a 5 min period of signal averaging was employed for each mass spectrum. To identify the molecular structure of each CL molecular species, product ion analysis of the selected ion was performed with Q1 operated at a unit resolution setting with a mass window of 0.7 Th. Shotgun lipidomics analyses of lipid molecular species of all other lipid classes were performed on a QqQ mass spectrometer (Thermo Electron TSQ Quantum Ultra, San Jose, CA) equipped with an electrospray ion source as previously described (27). All ESI/MS analyses of lipids were conducted by direct infusion employing a Harvard syringe pump at a flow rate of 4 μL/min. Typically, an 1 min period of signal averaging was employed for each mass spectrum, and a 2 min period of signal averaging was employed for each tandem MS spectrum. A mass resolution of 0.4 Th at half-peak width was used for both MS and tandem MS analyses performed by the QqQ mass spectrometer.

Data Processing

Each acquired mass spectrum using a QqTOF mass spectrometer was recalibrated using the theoretical m/z of T14:0 CL (619.4146 Th) and 18:0−22:6 GPEtn (790.5387 Th), which are present in every mass spectrum acquired from mouse myocardial lipid extracts, of sufficient abundance and not overlapped with other molecular species under experimental conditions. After recalibration, a mass accuracy of <10 ppm could be achieved (mass accuracy was evaluated by comparing the experimental m/z of multiple deprotonated CL species to their theoretical values). Quantitation of individual CL molecular species was achieved by comparing the total ion intensity (I_{total}) of an individual CL molecular species after ^{13}C deisotoping (see below) to that of the selected internal standard (i.e., T14:0 CL) as previously described (30). The total ion intensity (I_{total}) of an individual CL molecular species (M) was calculated from the peak intensity of its doubly charged plus-one isotopologue ($[M + 1 − 2H]^{2-}$) and its theoretical ^{13}C isotopic distribution. Briefly, the peak intensity of the $[M + 1 − 2H]^{2-}$ isotopologue (I_1) was determined from the mass spectrum. The peak intensities of the other isotopologues of this CL molecular species (M) including $[M − 2H]^{2-}$ (monoisotopic ion), $[M + 2 − 2H]^{2-}$, $[M + 3 − 2H]^{2-}$, and $[M + 4 − 2H]^{2-}$ were calculated from I_1. I_{total} was approximately the sum of these values as follows:

$$I_{total} = I_1 \left[92.42 / n + 1 + 5.41 \times 10^{-3}(n - 1) + 1.95 \times 10^{-5}(n - 1)(n - 2) + 5.3 \times 10^{-8}(n - 1)(n - 2)(n - 3) + ... \right] \tag{1}$$

where I_{total} is the deisotoped ion intensity of an individual CL molecular species (M) of interest, I_1 is the peak intensity of its $[M + 1 − 2H]^{2-}$ isotopologue, and n is the total carbon number in the species. Thus, the absolute quantity of an individual CL molecular species was determined as

$$[CL]_M = \left(\frac{I_{total,M}}{I_{total,T14:0}} \right) [CL]_{T14:0} \tag{2}$$

where $[CL]_M$ stands for the absolute quantity of the CL molecular species M in units of nanomoles per milligram of protein, $I_{total,M}$ is the total ion intensity of CL molecular species M, $I_{total,T14:0}$ is the total ion intensity of the CL internal standard (T14:0 CL), and $[CL]_{T14:0}$ is the absolute quantity of the T14:0 CL in units of nanomoles per milligram of protein which was added during lipid extraction. It should be emphasized that we chose to use the $[M + 1 − 2H]^{2-}$ isotopologue instead of the monoisotopic ion ($[M − 2H]^{2-}$) for quantitation because the $[M + 1 − 2H]^{2-}$ isotopologue is unique to CL molecular species under the experimental conditions whereas the monoisotopic ion may overlap with the molecular species of other lipid classes [e.g., the monoisotopic ion of 22:6−18:2−18:2−18:2 CL (m/z 747.477) overlaps with the monoisotopic ion of 16:0−18:1 GPGro (m/z 747.518)]. Moreover, in the case of the presence of a CL molecular species (M − 2) whose mass is two mass units less than M, I_1 should be replaced with the corrected ion peak intensity of the plus-one isotopologue of M. The correction can be calculated as follows:

$$I_{1(M)} = I'_{1(M)} - I_{3(M-2)} = I'_{1(M)} - \left(1.95 \times 10^{-5} \right) I_{1(M-2)}(n - 1)(n - 2) \tag{3}$$

where $I'_{1(M)}$ is the measured peak intensity at the $[M − 2H + 1]^{2-}$ isotopologue of M, $I_{3(M-2)}$ is the peak intensity of the plus-three isotopologue (i.e., $[(M − 2) − 2H + 3]^{2-}$) of M − 2 CL molecular species, and $I_{1(M-2)}$ is the peak intensity of the plus-one isotopologue of M − 2 CL molecular species; n is the total carbon number in the CL molecular species (M − 2), which should be identical to the carbon number in the molecular species of M. A Microsoft Excel

macro-based program was composed to perform peak selection, data transfer, and all aforementioned calculations.

Miscellaneous

Protein concentration was determined with a bicinchoninic acid protein assay kit (Pierce, Rockford, IL) using bovine serum albumin as a standard. Data from biological samples were normalized to the protein content, and all data are presented as the mean $\pm$ SEM of $n \geq 4$ for lipid analyses. Statistical differences between mean values were determined by the Wilcoxon rank-sum test.

RESULTS

Dramatic Alterations in CL Molecular Species in Diabetic Myocardium Induced by STZ Treatment

To further identify the changes in cellular CL molecular species (including low abundance components) induced by diabetes and the potential roles of the altered CL content and molecular composition in the diabetic state, we recently developed a novel shotgun lipidomics approach for direct analysis of individual CL molecular species (30). By using this novel shotgun lipidomics approach, CL molecular species present in less than 0.1 mol % of the total CL content in mouse myocardium can be readily analyzed by exploiting the unique doubly anionic charge of CL molecular species (30). First, using this approach, we have confirmed our previous observations of the substantial depletion of the most abundant CL molecular species present in heart (compare the ion peaks at m/z 723.477 and 724.485 of Figure 1, corresponding to T18:2 CL and 18:1−18:2−18:2−18:2 CL, respectively) in the diabetic state for 6 weeks. The identities of these major molecular species were confirmed by both accurate mass (Figure 1) and tandem MS analyses (spectrum not shown) as previously described (30).

In contrast to the myocardial CL profile of control mice in which T18:2 CL and 18:1−18:2 −18:2−18:2 CL are the predominant molecular species (Figure 1A), the CL molecular species profile in diabetic myocardium is dramatically altered as evidenced by a shift into the mass region beyond the ion at m/z 748.485 (corresponding to 18:1−18:2−18:2−22:6 CL) (Figure 1B). For example, peak intensities of the ion clusters at m/z 748.485, 761.493, 772.485, 784.485, and 795.477 are markedly increased in STZ-induced diabetes (Figure 1B compared to Figure 1A). Collectively, these results show substantial alterations in CL molecular species and indicate a dramatic change in CL metabolism in the mitochondrial inner membrane in the diabetic state.

Dramatic Depletion of Myocardial CL Content and Altered CL Molecular Species Occur within Days after Induction of the Diabetic State

To demonstrate the temporal relationship between alterations in myocardial CL content, CL molecular species composition, and dysfunctional lipid metabolism (e.g., TG accumulation) in the diabetic state, we determined the temporal course of the changes in CL content and molecular species composition in mouse myocardium at the earliest stages of the diabetic state after STZ injection. Shotgun lipidomics analyses demonstrated selective changes in individual CL molecular species in heart at the earliest stages of diabetes. For example, the quantities of CL molecular species containing 16:1 FA (e.g., 16:1−18:2−18:2−18:2 CL, the doubly charged ion at m/z 710.469) were significantly decreased (i.e., over 20 mol %, $p < 0.0001$) as early as 5 days after the induction of diabetes (Figure 2A). However, the quantities of the other CL molecular species in diabetic mouse myocardium did not significantly change within the first 5 days after STZ treatment (Figure 2A). The quantities of CL molecular species containing fatty acyl chains other than 22:6 FA (e.g., T18:2 CL, 18:1−18:2−18:2−18:2 CL, 18:2−18:2 −18:2−20:4 CL, and 18:2−18:2−18:2−20:3 CL at m/z 723.477, 724.485, 735.477, and 736.485,

respectively) are substantially decreased at approximately 6 days after the onset of diabetes relative to controls (e.g., Figure 2A). Specifically, the content of total CL, 18:2−18:2−18:2 −20:3 CL, T18:2 CL, and 16:1−18:2−18:2−18:2 CL was reduced by 20, 28, 35, 55 mol %, respectively, 6 days after STZ injection in comparison to controls. The quantities of these CL molecular species do not further decrease significantly in the diabetic hearts between 6 and 40 days as examined (e.g., Figure 2A).

In sharp contrast to the decreased quantities of CL molecular species containing fatty acyl chains other than 22:6 FA, the quantities of all measurable CL molecular species containing 22:6 FA were increased at day 6. The magnitude of the quantity elevations of these 22:6-containing CL molecular species correlated with the numbers of 22:6 chains present (Figure 2B). Increases in the quantities of CL molecular species at the ion clusters of m/z 760.485 (18:2 −18:2−20:3−22:6 CL), m/z 771.477 (18:2−18:2−22:6−22:6 CL), m/z 784.485 (18:2−20:3−22:6 −22:6 CL), and m/z 795.477 (18:2−22:6−22:6−22:6 CL) were observable approximately 6 days after the onset of diabetes relative to controls. The increases were statistically significant between 6 and 20 days ($p < 0.01$) and were further amplified after 20 days following STZ treatment for all of these CL molecular species ($p < 0.001$) (Figure 2B). Particularly remarkable was the 16-fold increase in 18:2−22:6−22:6−22:6 CL at 40 days after STZ treatment. Thus, alterations in CL molecular species occurred at the very earliest stages of the diabetic state (6 days), and alterations in content were substantially different for different CL molecular species.

In addition to changes in individual CL molecular species, the temporal course of alterations in fatty acyl chains in the CL pool present in diabetic myocardium relative to controls was also intriguing (Figure 3). For example, the composition of 16:1 FA in total fatty acyl chains of CL was substantially decreased (approximately 20 mol %) after 5 day STZ treatment, was reduced by over 60 mol % after 6 day STZ treatment, and was almost nonexistent after 40 days of diabetes. The content of 18:1 FA in the mouse myocardial CL pool was significantly decreased initially ($p < 0.01$) but became increased after 20 days following STZ treatment. The content of 18:2 FA did not decrease until 6 days after STZ treatment and reached a minimum approximately 10 days after the onset of diabetes. Finally, a significant increase in the content of 22:6 FA in mouse myocardium was manifest at 6 days after STZ treatment ($p < 0.01$).

To substantiate the disparate changes in different CL molecular species containing 22:6 FA, we performed neutral loss scanning of 155.1 units [corresponding to the 22:6 ketene lost from doubly charged CL molecular ions, which is specific for the CL molecular species containing 22:6 acyl chains as previously described (30)] (Figure 4). These tandem mass spectra semiquantitatively represent the profiles of CL molecular species containing 22:6 FA moieties whose ratiometric intensities can be compared between control and diabetic states. Thus, independent approaches showed CL content increases in molecular species containing 22:6 FA at day 40 of diabetes.

Dramatic Alterations in Myocardial CL Molecular Species in a Model of Type II Diabetics (i.e., Insulin-Resistant, Leptin-Deficient ob/ob Mice)

To compare the findings observed in the diabetic type I model (i.e., STZ-treated mouse hearts), we next used the newly developed shotgun lipidomics approach to analyze individual CL molecular species in myocardial lipid extracts of *ob*/*ob* mice (i.e., an animal model of type II diabetes, or insulin resistance) at 2−4 months of age. It has been well-established that *ob*/*ob* mice become insulin resistant approximately at 2 months of age and develop hyperglycemia between 3 and 4 months of age (see refs 35 and 36 for reviews).

Shotgun lipidomics analyses demonstrated alterations in myocardial CL molecular species profiles of the *ob*/*ob* mice at 4 months of age that was almost identical to that observed in mice after STZ treatment for 40 days (compare Figure 5B to Figure 1B). Specifically, a 60 and 45

mol % reduction in abundant CL content as indicated by the decreased peak intensities of the ions at m/z 723.477 and 724.485 corresponding to T18:2 CL and 18:1−18:2−18:2−18:2 CL, respectively, was manifest whereas remarkable increases in the quantities of CL molecular species corresponding to the ion clusters at m/z 760.483, 771.477, 784.485, and 795.477 were present (indicated with asterisks). A reduction of total CL content from 16.4 ± 1.0 to 14.5 ± 0.7 nmol/mg of protein at 4 months of age ($p < 0.05$) was present.

The quantities of different CL molecular species were distinctly altered in *ob/ob* mouse myocardium in comparison to their WT counterparts (Figure 6). For example, a 7-fold decrease in the content in T18:2 CL was manifested whereas a 13-fold increase in the content of 18:2 −22:6−22:6−22:6 CL was observed in *ob/ob* mouse myocardium relative to that in WT mice at 4 months of age. Furthermore, alterations in CL metabolism occur at the youngest age (i.e., 2 months) examined (Figure 6). Specifically, higher quantities of 16:1−18:2−18:2−18:2 CL (0.12 ± 0.02 vs 0.08 ± 0.01 nmol/mg of protein), 18:2−18:2−18:2−20:3 CL (0.89 ± 0.05 vs 0.42 ± 0.02 nmol/mg of protein), and 18:2−18:2−20:3−22:6 CL (0.27 ± 0.02 vs 0.12 ± 0.01 nmol/mg of protein) in *ob/ob* mouse myocardium relative to WT mice at 2 months of age were determined. It should be pointed out that analysis of temporal alterations in CL molecular species revealed that the quantities of almost all CL molecular species in WT mouse myocardium increase with aging. The biological mechanism and physiological impact of this age-dependent increase in the content change of CL in insulin-resistant type II diabetes is beyond the scope of this study but needs to be further investigated in the future. Collectively, these results are similar to changes in the type I model of diabetes, providing a unifying link between mitochondrial dysfunction in these two diabetic disease states.

Depletion of CL Content and Altered CL Molecular Species Precede the Accumulation of TG Content in STZ-Induced Diabetic Mouse Myocardium

One prominent chemical feature of diabetic cardiomyopathy is the accumulation of TG content in diabetic myocardium. To demonstrate the temporal relationship between alterations in myocardial CL content and molecular species composition and mitochondrial dysfunction, the quantity of TG and alterations in molecular species composition of TG in the diabetic state were quantified and compared to the temporal course of CL alterations. Alterations in CL molecular species profiles in the STZ-induced animal model preceded changes in the content and composition of individual TG molecular species (Figure 7A). Specifically, total TG content was significantly increased in STZ-induced diabetic mouse myocardium after STZ treatment for 10 days and was substantially increased thereafter (Figure 7A). Two-dimensional mass spectrometric analyses did not show any changes in TG molecular species profiles in diabetic myocardium after 5 day onset of diabetes and demonstrated that alterations in TG molecular species profiles in STZ-induced diabetic myocardium did not become apparent until 10 days after STZ treatment examined, which was similar to those previously described (6). These results indicated that loss of CL content and altered CL molecular species preceded the accumulation of TG content and altered TG molecular species in STZ-induced diabetic mouse myocardium.

Alterations in CL Metabolism Parallel the Accumulation of TG Content in ob/ob Mouse Myocardium

To identify the temporal relationship between altered CL metabolism and the accumulation of TG content in *ob/ob* mouse myocardium, we compared myocardial TG content and molecular species composition in *ob/ob* mice to their wild-type (WT) counterparts. Myocardial TG content in *ob/ob* mice was increased from 27.2 ± 1.9 to 50.3 ± 3.2 nmol/mg of protein at 2 months of age (the youngest age examined) (Figure 7B). Although myocardial TG quantities in both *ob/ob* and WT mice decreased from 2 to 4 months of age, the relative increase of TG content in *ob/ob* vs WT changed considerably (Figure 7B). For example, relative increases

from 187 to 312 mol % of TG content at 2 and 4 months of age, respectively, were manifested (Figure 7B).

Two-dimensional MS analyses of TG molecular species [which was comprised of neutral loss scanning of all potential building blocks of TG (i.e., naturally occurring fatty acids) as previously described (27,37)] demonstrated multiple changes in myocardial TG molecular species present in *ob/ob* mice relative to WT mice. First, the total ion current (TIC) chromatogram constituted from the neutral loss scanning of fatty acids demonstrated that the composition of the individual fatty acyl moiety in myocardial TG molecular species in *ob/ob* mice was quite different from that in WT mice (Figure 8). For example, the TIC ratio of 16:0, 18:2, and 18:1 FA in myocardial TG of WT mice was approximately 1:1.1:1.1 (Figure 8A) whereas this ratio in *ob/ob* mice was 1:1.4:1.9 (Figure 8B).

Next, the ion clusters greater than m/z 880 in traces obtained from the NL scanning of 14:0, 16:0, and 16:1 FA were significantly increased ($p < 0.01$) in myocardial TG molecular species in *ob/ob* mice (Figure 9B) in comparison to WT mice (Figure 9A). This observation indicated the increased incorporation of longer fatty acyl chain(s) (e.g., 22:6 FA) into TG molecular species in *ob/ob* mouse myocardium relative to control. For example, the myocardial TG molecular species containing 22:6 FA was increased from 1.9 ± 0.1 nmol/mg of protein in WT mice to 2.4 ± 0.2 nmol/mg of protein in *ob/ob* mice at 2 months of age ($p < 0.05$).

Finally, the peak intensity ratio of the higher m/z ion vs the lower m/z ion in the same cluster of myocardial TG molecular species was significantly larger in *ob/ob* mice than that in WT mice. For example, this ratio between the predominant TG species at m/z 889.7 (mainly corresponding to 18:1−18:1−18:2 TG) and 885.7 (mainly corresponding to 18:2−18:2−18:2 TG) in traces obtained from the NL scanning of 280.2 (18:2 FA) was 1.3 in *ob/ob* mice but only 0.6 in WT mice ($p < 0.001$). This result indicated the increased quantities of TG molecular species containing 18:1 FA in *ob/ob* mice in comparison to WT mice in accordance with the results of the TIC chromatogram. Collectively, these results indicated that depletion of abundant CL molecular species and alterations in molecular species relative composition paralleled the accumulation of TG content and altered TG molecular species in *ob/ob* mouse myocardium.

Alterations in GPA, GPGro, FFA, and Acyl-CoA Molecular Species Profiles Do Not Parallel the Alterations in CL Molecular Species Profiles in Diabetic Mouse Hearts

One biochemical mechanism potentially responsible for the depletion of abundant T18:2 CL molecular species and increases in content in CL molecular species containing 22:6 FA is alterations in the substrate precursor pools involved in CL de novo synthesis. A second is the abnormal remodeling of CL molecular species in diabetic states. Accordingly, the quantities of precursor substrates directly involved in CL synthesis (i.e., GPA and GPGro) as well as those involved in CL remodeling (e.g., FFA and acyl-CoA) were examined. Some precursor pools significantly changed in both STZ-treated and *ob/ob* mice in comparison to controls [e.g., from 1.8 ± 0.1 to 1.3 ± 0.1 nmol of GPGro/mg of protein ($p < 0.001$), 36.6 ± 2.7 to 35.7 ± 1.8 pmol of GPA/mg of protein, and 25.3 ± 1.1 to 30.9 ± 2.1 nmol of FFA/mg of protein ($p < 0.01$) from controls to STZ-treated mice; changed from 1.7 ± 0.1 to 1.4 ± 0.1 nmol of GPGro/mg of protein ($p < 0.01$), 36.7 ± 2.8 to 58.9 ± 9.3 pmol of GPA/mg of protein ($p < 0.001$), and 22.2 ± 1.6 to 31.8 ± 2.2 nmol of FFA/mg of protein ($p < 0.01$) from 4 month WT mice to *ob/ob* mice], and corresponding alterations in molecular species composition were also identified in each pool (Figure 10). Surprisingly, there was no substantial loss of GPGro, GPA, and FFA molecular species containing 18:2 FA (Figure 10) as well as 18:2 acyl-CoA (data not shown), but significant increases in the content of 18:2−18:2 GPA ($p < 0.01$) were present (Figure 10B). No increases in the quantities of 22:6 FFA (Figure 10C) and 22:6 acyl-CoA (data not shown) or the quantities of 22:6 FA-containing GPA and GPGro were present. In both control and

diabetic hearts 22:6 FA-containing molecular species were present in minor amounts (less than 5 mol % except in FFA). These results indicate that alterations in the precursors for CL de novo synthesis did not contribute to the abundance of 22:6 FA-containing CL molecular species present in the diabetic state.

DISCUSSION

Through the use of our recently developed enhanced shotgun lipidomics approach for analysis of CL molecular species, the current study demonstrates dramatic changes in CL content and molecular species composition that occurred at the very earliest stages of the diabetic state in two independent models of diabetes. In the case of STZ-induced diabetes, depletion of the major 18:2 FA-containing CL molecular species occurred within days of induction of the diabetic state, and normally low abundance molecular species (e.g., 22:6 FA-containing CL moieties) rapidly accumulated during the progression of the diabetic state. Alterations in CL content and molecular species composition have profound effects on mitochondrial function manifest as a profound cardiomyopathy as demonstrated in the genetic disorder, Barth syndrome, which is due to defective CL remodeling by the enzyme tafazzin. Genetic alterations in tafazzin result in pathological changes in both the content and molecular composition of CL in mitochondrial membranes and lead to dramatic changes in mitochondrial function. Collectively, the current results, in analogy to Barth syndrome, have established a link between altered CL mitochondrial membrane composition, membrane dynamics, function, and cardiac bioenergetics.

The dramatic loss of abundant T18:2 CL molecular species in diabetic myocardium induced by STZ treatment was determined from our previous work using conventional shotgun lipidomics and confirmed by the novel shotgun lipidomics approach used here. Moreover, the doubly negatively charged state of CL molecular species facilitated unambiguous identification of their molecular composition through the use of the $[M - 2H + 1]^{2-}$ isotopologues found only in doubly charged species under experimental conditions. Through combining these approaches, the extraordinary sensitivity of this technique led to identification of over 50 CL molecular species, some of which represented <0.1% of the total CL content. The actual number of CL molecular species likely approaches 100 or more as this calculation does not individually consider the number of regioisomers, enantiomers, and diasteromers produced by the presence of the three chiral carbons in the glycerol moieties in CL. In addition, the presence of lysoCL molecular species in the lipid extracts was also readily detected as previously described (30), but represented <1% of total CL content in both the control and diabetic state. Due to the lack of a suitable internal standard for quantitation of lysoCL molecular species, the altered content of lysoCL induced by diabetes was not quantified. Collectively, this novel shotgun lipidomics analysis demonstrated that CL molecular species were dramatically remodeled during the development and progression of both type I and type II diabetes.

Next, we were interested in determining if the available data provided insight into the molecular pathways by which 22:6 FA-containing CL molecular species accumulated. To this end, we first examined the acyl chain composition of biosynthetic precursors of CL in the diabetic state. No evidence for the accumulation of 22:6 FA-containing molecular species in the CL precursor pool was manifest. However, our previous studies have demonstrated that mitochondrial phospholipids in murine myocardium contain large amounts of 22:6 FA-containing molecular species at their *sn*-2 position (6,38). Mitochondrial phospholipases are known to be activated in the diabetic state (5). Thus, it seems likely that the activation of phospholipases in the diabetic state leads to the generation of monolysoCL followed by direct transacylation of the 22:6 FA from phospholipid pools to monolysoCL by tafazzin as recently characterized in detail (24, 39). Although we cannot exclude the presence of compartmentalized pools of 22:6 CoA and selective monolysoCL acyltransferases, we believe this possibility is unlikely since no increase

in 22:6 CoA (data not shown) could be identified and other classes containing increased 22:6 FA groups were not found. Thus, it seems likely that the activation of mitochondrial phospholipases (e.g., iPLA$_2\beta$ or iPLA$_2\gamma$) followed by the specific transacylation of the predominant acyl chain (e.g., 22:6 FA) in mitochondrial phospholipids (i.e., GPCho and GPEtn) led to both the observed CL depletion and acyl chain remodeling. However, we specifically point out that although we have determined the content and molecular species composition of FFA and acyl-CoA in myocardial homogenates, we cannot exclude the effects of metabolic compartmentation which may significantly affect CL biosynthesis.

Changes in CL molecular species composition and content perturb the biophysical environment of mitochondrial membranes, which alters the mitochondrial membrane potential and activities of transmembrane enzymes, and result in changes in mitochondrial dynamics and bioenergetics. It is well-known that the optimal functions of many mitochondrial proteins (e.g., cytochrome *c*, cytochrome *c* oxidase, and ATP synthase) depend on the association of these proteins with specific tetra 18:2 CL molecular species profiles (13–15,40–44). Therefore, it can be anticipated that these changes in CL molecular species profiles and quantities in diabetic myocardium contribute to the mitochondrial dysfunction manifest in diabetic hearts.

It should be pointed out that the alterations in CL content and molecular species composition occur as early as 5 days after STZ injection. To the best of our knowledge, no significant changes in mitochondrial morphology or function have previously been reported within this time frame. Since substantial changes in CL begin to manifest themselves at this early time point, it is likely that alterations in CL are very sensitive biomarkers for mitochondrial alterations in the diabetic state or moreover precipitate mitochondrial dysfunction itself in diabetes.

Accumulation of TG content is one of the chemical hallmarks of diabetic cardiomyopathy. Shotgun lipidomics analyses demonstrate the accumulation of TG content and changes in TG molecular species profiles in both type I and type II diabetic hearts. The present study clearly identifies changes in CL molecular species metabolism that can precipitate mitochondrial dysfunction and compromise the ability of mitochondria to effectively remove the lipid burden presented to hearts in the diabetic state. The likely mechanism underlying this defect in TG removal is the inefficient function of the electron transport chain in the presence of nonphysiological CL concentrations and molecular species leading to an increase in negative redox potential and a deficiency in the flux of mitochondrial fatty acid β-oxidation.

In summary, through use of our newly developed enhanced shotgun lipidomics approach based on the unique chemical features of cardiolipin molecular species, we have demonstrated that abundant CL molecular species content depletion and substantial CL molecular species remodeling precede the lipotoxic hallmarks of diabetic cardiomyopathy (e.g., TG accumulation). Through exploiting the power of lipidomics, new insights into the chemical mechanisms of diabetic cardiomyopathy have been made. Similarly, the approaches presented herein can be used to identify treatment efficacy of pharmacological reagents and identify novel biomarkers predictive of mitochondrial function and the severity of the diabetic state.

REFERENCES

1. Lopaschuk GD, Russell JC. Myocardial function and energy substrate metabolism in the insulin-resistant JCR:LA corpulent rat. J. Appl. Physiol 1991;71:1302–1308. [PubMed: 1757353]

2. Han X, Abendschein DR, Kelley JG, Gross RW. Diabetes-induced changes in specific lipid molecular species in rat myocardium. Biochem. J 2000;352:79–89. [PubMed: 11062060]

3. Zhou YT, Shimabukuro M, Lee Y, Koyama K, Higa M, Ferguson T, Unger RH. Enhanced de novo lipogenesis in the leptin-unresponsive pancreatic islets of prediabetic Zucker diabetic fatty rats: role in the pathogenesis of lipotoxic diabetes. Diabetes 1998;47:1904–1908. [PubMed: 9836522]

4. Kraegen EW, Cooney GJ, Ye JM, Thompson AL, Furler SM. The role of lipids in the pathogenesis of muscle insulin resistance and beta cell failure in type II diabetes and obesity. Exp. Clin. Endocrinol. Diabetes 2001;109(Suppl 2):S189–S201. [PubMed: 11460570]

5. Su X, Han X, Mancuso DJ, Abendschein DR, Gross RW. Accumulation of long-chain acylcarnitine and 3-hydroxy acylcarnitine molecular species in diabetic myocardium: identification of alterations in mitochondrial fatty acid processing in diabetic myocardium by shotgun lipidomics. Biochemistry 2005;44:5234–5245. [PubMed: 15794660]

6. Han X, Yang J, Cheng H, Yang K, Abendschein DR, Gross RW. Shotgun lipidomics identifies cardiolipin depletion in diabetic myocardium linking altered substrate utilization with mitochondrial dysfunction. Biochemistry 2005;44:16684–16694. [PubMed: 16342958]

7. Unger RH. Lipotoxic diseases. Annu. Rev. Med 2002;53:319–336. [PubMed: 11818477]

8. Hung T, Sievenpiper JL, Marchie A, Kendall CW, Jenkins DJ. Fat versus carbohydrate in insulin resistance, obesity, diabetes and cardiovascular disease. Curr. Opin. Clin. Nutr. Metab. Care 2003;6:165–176. [PubMed: 12589186]

9. Finck BN, Han X, Courtois M, Aimond F, Nerbonne JM, Kovacs A, Gross RW, Kelly DP. A critical role for PPARRα-mediated lipotoxicity in the pathogenesis of diabetic cardiomyopathy: modulation by dietary fat content. Proc. Natl. Acad. Sci. U.S.A 2003;100:1226–1231. [PubMed: 12552126]

10. Finck BN, Lehman JJ, Leone TC, Welch MJ, Bennett MJ, Kovacs A, Han X, Gross RW, Kozak R, Lopaschuk GD, Kelly DP. The cardiac phenotype induced by PPARRα overexpression mimics that caused by diabetes mellitus. J. Clin. Invest 2002;109:121–130. [PubMed: 11781357]

11. Kelley DE. Skeletal muscle triglycerides: an aspect of regional adiposity and insulin resistance. Ann. N.Y. Acad. Sci 2002;967:135–145. [PubMed: 12079843]

12. Schlame M, Haldar D. Cardiolipin is synthesized on the matrix side of the inner membrane in rat liver mitochondria. J. Biol. Chem 1993;268:74–79. [PubMed: 8380172]

13. Mandieau V, Martin I, Ruysschaert JM. Interaction between cardiolipin and the mitochondrial presequence of cyto-chrome c oxidase subunit IV favours lipid mixing without destabilizing the bilayer structure. FEBS Lett 1995;368:15–18. [PubMed: 7615071]

14. Zhang M, Mileykovskaya E, Dowhan W. Gluing the respiratory chain together. Cardiolipin is required for supercomplex formation in the inner mitochondrial membrane. J. Biol. Chem 2002;277:43553–43556. [PubMed: 12364341]

15. Pfeiffer K, Gohil V, Stuart RA, Hunte C, Brandt U, Greenberg ML, Schagger H. Cardiolipin stabilizes respiratory chain supercomplexes. J. Biol. Chem 2003;278:52873–52880. [PubMed: 14561769]

16. Vreken P, Valianpour F, Nijtmans LG, Grivell LA, Plecko B, Wanders RJ, Barth PG. Defective remodeling of cardiolipin and phosphatidylglycerol in Barth syndrome. Biochem. Biophys. Res. Commun 2000;279:378–382. [PubMed: 11118295]

17. Schlame M, Towbin JA, Heerdt PM, Jehle R, DiMauro S, Blanck TJ. Deficiency of tetralinoleoyl-cardiolipin in Barth syndrome. Ann. Neurol 2002;51:634–637. [PubMed: 12112112]

18. Valianpour F, Wanders RJ, Overmars H, Vreken P, Van Gennip AH, Baas F, Plecko B, Santer R, Becker K, Barth PG. Cardiolipin deficiency in X-linked cardioskeletal myopathy and neutropenia (Barth syndrome, MIM 302060): a study in cultured skin fibroblasts. J. Pediatr 2002;141:729–733. [PubMed: 12410207]

19. Barth PG, Valianpour F, Bowen VM, Lam J, Duran M, Vaz FM, Wanders RJ. X-linked cardioskeletal myopathy and neutropenia (Barth syndrome): an update. Am. J. Med. Genet. A 2004;126:349–354. [PubMed: 15098233]

20. Gu Z, Valianpour F, Chen S, Vaz FM, Hakkaart GA, Wanders RJ, Greenberg ML. Aberrant cardiolipin metabolism in the yeast taz1 mutant: a model for Barth syndrome. Mol. Microbiol 2004;51:149–158. [PubMed: 14651618]

21. Hauff KD, Hatch GM. Cardiolipin metabolism and Barth Syndrome. Prog. Lipid Res 2006;45:91–101. [PubMed: 16442164]

22. Li G, Chen S, Thompson MN, Greenberg ML. New insights into the regulation of cardiolipin biosynthesis in yeast: Implications for Barth syndrome. Biochim. Biophys. Acta. 2006(doi:10.1016/j.bbalip.2006.1006.1007)

23. Schlame M, Ren M. Barth syndrome, a human disorder of cardiolipin metabolism. FEBS Lett 2006;580:5450–5455. [PubMed: 16973164]

24. Xu Y, Kelley RI, Blanck TJ, Schlame M. Remodeling of cardiolipin by phospholipid transacylation. J. Biol. Chem 2003;278:51380–51385. [PubMed: 14551214]

25. Vaz FM, Houtkooper RH, Valianpour F, Barth PG, Wanders RJ. Only one splice variant of the human TAZ gene encodes a functional protein with a role in cardiolipin metabolism. J. Biol. Chem 2003;278:43089–43094. [PubMed: 12930833]

26. Han X, Gross RW. Global analyses of cellular lipidomes directly from crude extracts of biological samples by ESI mass spectrometry: a bridge to lipidomics. J. Lipid Res 2003;44:1071–1079. [PubMed: 12671038]

27. Han X, Yang J, Cheng H, Ye H, Gross RW. Towards fingerprinting cellular lipidomes directly from biological samples by two-dimensional electrospray ionization mass spectrometry. Anal. Biochem 2004;330:317–331. [PubMed: 15203339]

28. Han X, Gross RW. Shotgun lipidomics: Electrospray ionization mass spectrometric analysis and quantitation of the cellular lipidomes directly from crude extracts of biological samples. Mass Spectrom. Rev 2005;24:367–412. [PubMed: 15389848]

29. Han X, Gross RW. Shotgun lipidomics: multidimensional mass spectrometric analysis of cellular lipidomes. Expert Rev. Proteomics 2005;2:253–264. [PubMed: 15892569]

30. Han X, Yang K, Yang J, Cheng H, Gross RW. Shotgun lipidomics of cardiolipin molecular species in lipid extracts of biological samples. J. Lipid Res 2006;47:864–879. [PubMed: 16449763]

31. Gross RW. High plasmalogen and arachidonic acid content of canine myocardial sarcolemma: a fast atom bombardment mass spectroscopic and gas chromatography-mass spectroscopic characterization. Biochemistry 1984;23:158–165. [PubMed: 6419772]

32. Bligh EG, Dyer WJ. A rapid method of total lipid extraction and purification. Can. J. Biochem. Physiol 1959;37:911–917. [PubMed: 13671378]

33. Golovko MY, Murphy EJ. An improved method for tissue long-chain acyl-CoA extraction and analysis. J. Lipid Res 2004;45:1777–1782. [PubMed: 15210839]

34. Kalderon B, Sheena V, Shachrur S, Hertz R, Bar-Tana J. Modulation by nutrients and drugs of liver acyl-CoAs analyzed by mass spectrometry. J. Lipid Res 2002;43:1125–1132. [PubMed: 12091497]

35. Herberg L, Coleman DL. Laboratory animals exhibiting obesity and diabetes syndromes. Metabolism 1977;26:59–99. [PubMed: 834144]

36. Bray GA, York DA. Hypothalamic and genetic obesity in experimental animals: an autonomic and endocrine hypothesis. Physiol. Rev 1979;59:719–809. [PubMed: 379887]

37. Han X, Gross RW. Quantitative analysis and molecular species fingerprinting of triacylglyceride molecular species directly from lipid extracts of biological samples by electrospray ionization tandem mass spectrometry. Anal. Biochem 2001;295:88–100. [PubMed: 11476549]

38. Han X, Cheng H, Mancuso DJ, Gross RW. Caloric restriction results in phospholipid depletion, membrane remodeling and triacylglycerol accumulation in murine myocardium. Biochemistry 2004;43:15584–15594. [PubMed: 15581371]

39. Xu Y, Malhotra A, Ren M, Schlame M. The enzymatic function of tafazzin. J. Biol. Chem. 2006(in press)

40. Schlame M, Rua D, Greenberg ML. The biosynthesis and functional role of cardiolipin. Prog. Lipid Res 2000;39:257–288. [PubMed: 10799718]

41. Iverson SL, Orrenius S. The cardiolipin-cytochrome c interaction and the mitochondrial regulation of apoptosis. Arch. Biochem. Biophys 2004;423:37–46. [PubMed: 14989263]

42. Hatch GM. Cell biology of cardiac mitochondrial phospholipids. Biochem. Cell Biol 2004;82:99–112. [PubMed: 15052331]

43. McMillin JB, Dowhan W. Cardiolipin and apoptosis. Biochim. Biophys. Acta 2002;1585:97–107. [PubMed: 12531542]

44. Chicco AJ, Sparagna GC. Role of cardiolipin alterations in mitochondrial dysfunction and disease. Am. J. Physiol. Cell. Physiol 2007;292:C33–C44. [PubMed: 16899548]
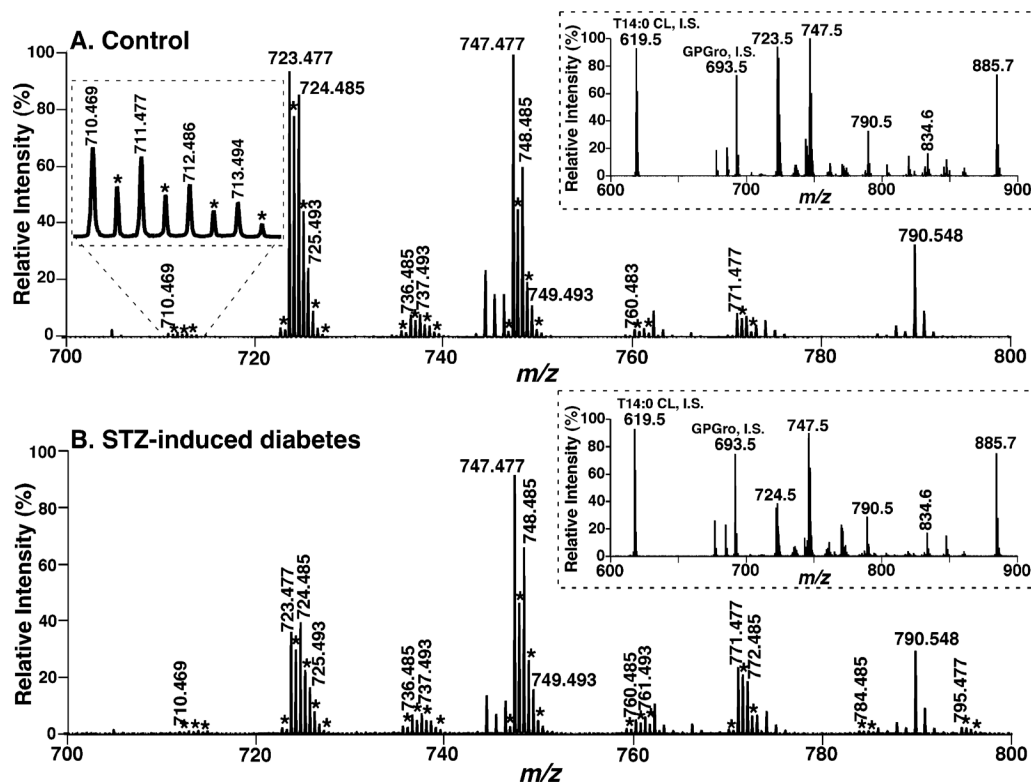
Figure 1.
Expanded negative-ion electrospray ionization mass spectra of myocardial lipid extracts from STZ-treated diabetic and control mice. Myocardial lipid extracts of control (panel A) and diabetic (after STZ treatment for 6 weeks, panel B) mice were prepared by a modified Bligh and Dyer procedure as described under Materials and Methods. Negative-ion ESI mass spectra were acquired by using a QqTOF mass spectrometer as described under Materials and Methods. Both spectra displayed have been normalized to the CL internal standard (see insets). The asterisks indicate the majority of the doubly charged CL plus-one isotopologues whose ion peak intensities are utilized to quantify individual CL molecular species as described under Materials and Methods. Other unlabeled ion peaks correspond to deprotonated molecular species of other anionic phospholipids and ethanolamine glycerophospholipids. The insets on the right side show the extended mass spectra that display the internal standards and other major anionic phospholipids. The inset on the left side of panel A shows an enlarged ion cluster that displays the peak resolution and peak shape of the ions and their isotopologues of low abundance CL molecular species.
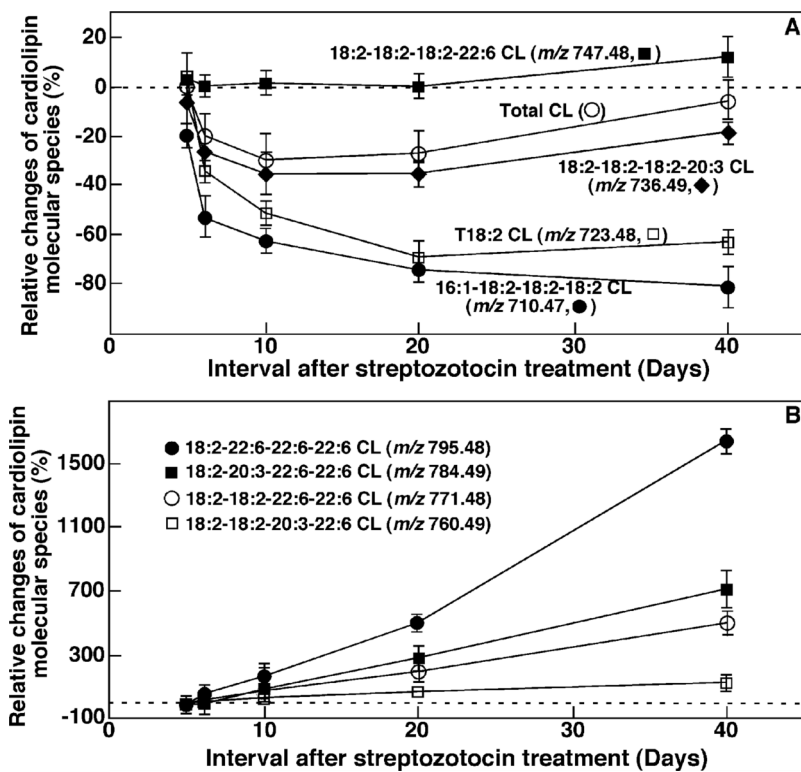
Figure 2.
Temporal changes in the quantities of selected CL molecular species in type I diabetic myocardium after STZ treatment. Lipid extracts of mouse myocardium at different time intervals after STZ treatment (as indicated) were prepared by using a modified Bligh and Dyer method. Relative changes of individual CL molecular species were calculated in comparison to controls. Each data point represents mean ± SEM from at least four different animals.
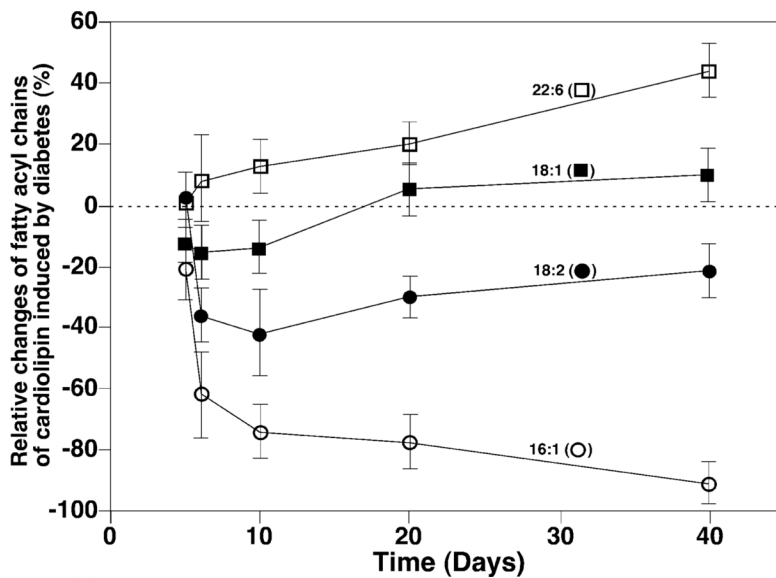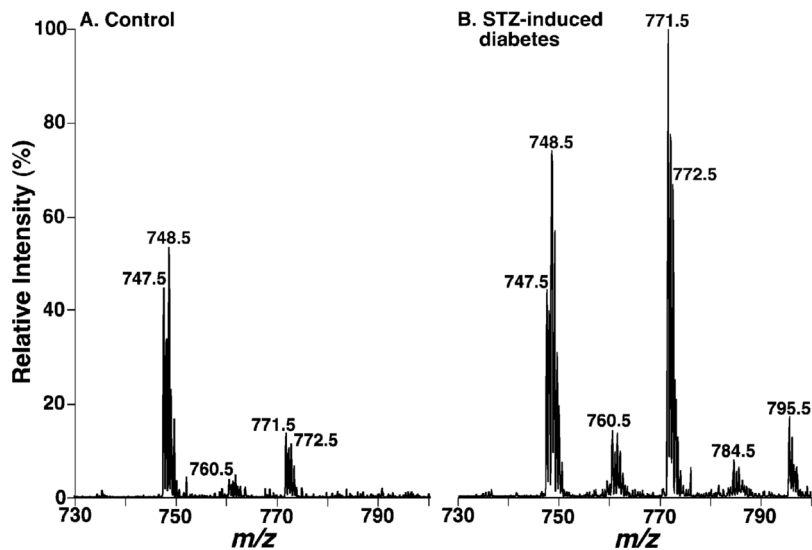
Figure 3.
Temporal course of changes of selected fatty acyl components in the cardiolipin pool in diabetic mouse myocardium after STZ treatment. The relative content changes of the selected individual fatty acyl chains (as indicated) of CL were calculated from the determined quantities of individual CL molecular species. Relative changes of individual fatty acyl chains were calculated in comparison to controls, and each data point represents mean ± SEM from at least four different animals.

Figure 4.
Dramatic changes of cardiolipin molecular species containing docosahexaenoate (22:6 FA) in STZ-induced diabetic mouse myocardium relative to controls. Lipid extracts were prepared by using a modified Bligh and Dyer method as described under Materials and Methods. CL molecular species containing 22:6 FA are profiled by neutral loss of 155.1 units (corresponding to the loss of a 22:6 ketene from doubly charged CL molecular species). For negative-ion tandem mass spectrometry in the neutral loss mode by using a QqQ mass spectrometer, both first and third quadrupoles were coordinately scanned with a mass difference (i.e., neutral loss) of 155.1 units from doubly charged CL molecular species while the second quadruple was used as a collision cell. The spectra are normalized to the CL ion peak at m/z 747.5 which was not significantly changed as determined by primary ions (Figure 1). The spectra indicate the dramatic increase of CL molecular species containing 22:6 FA in diabetic mouse myocardium.
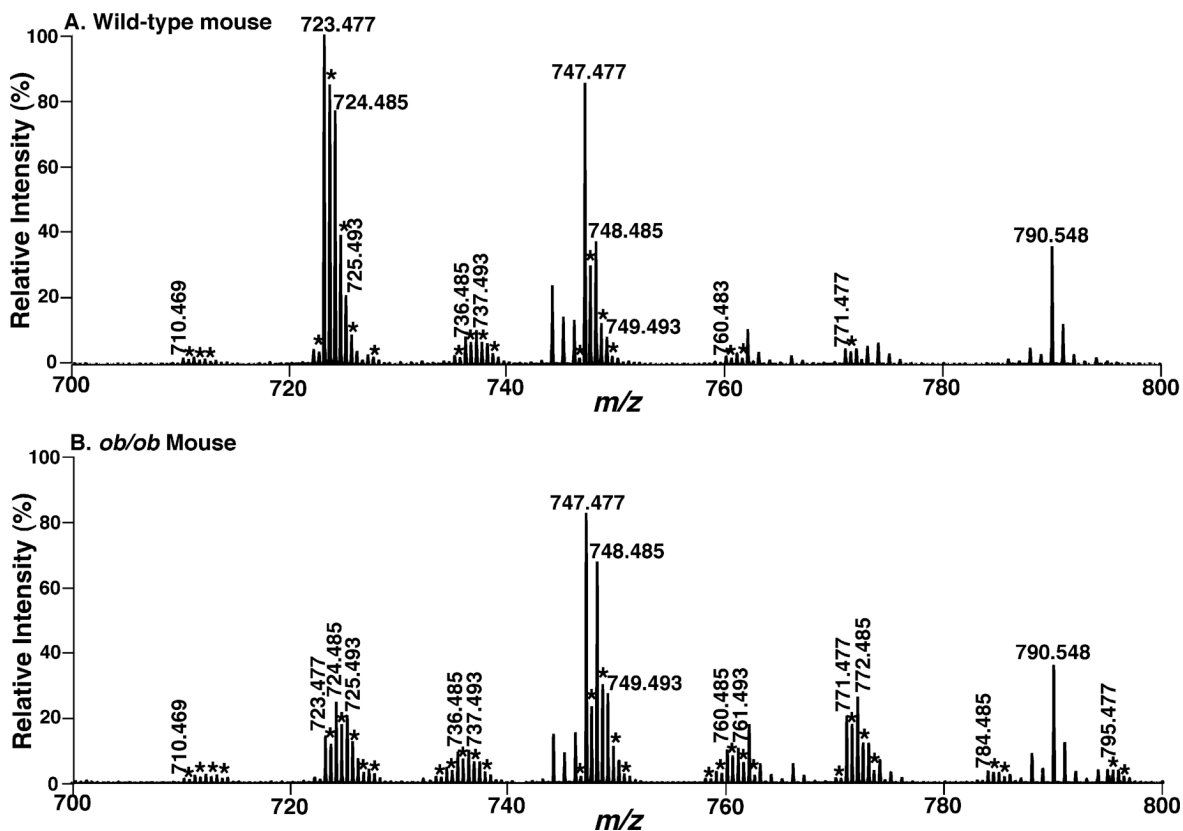
Figure 5.
Expanded negative-ion electrospray ionization mass spectra of myocardial lipid extracts from *ob*/*ob* and control mice. Myocardial lipid extracts of wild-type (panel A) and *ob*/*ob* (4 months of age, panel B) mice were prepared by a modified Bligh and Dyer procedure as described under Materials and Methods. Negative-ion ESI mass spectra were acquired by using a QqTOF mass spectrometer as described under Materials and Methods. Both spectra displayed have been normalized to the CL internal standard (which is not included in the spectra). The asterisks indicate the majority of the doubly charged CL plus-one isotopologues whose ion peak intensities are utilized to quantify individual CL molecular species as described under Materials and Methods. Other unlabeled ion peaks correspond to deprotonated molecular species of other anionic phospholipids and ethanolamine glycerophospholipids.
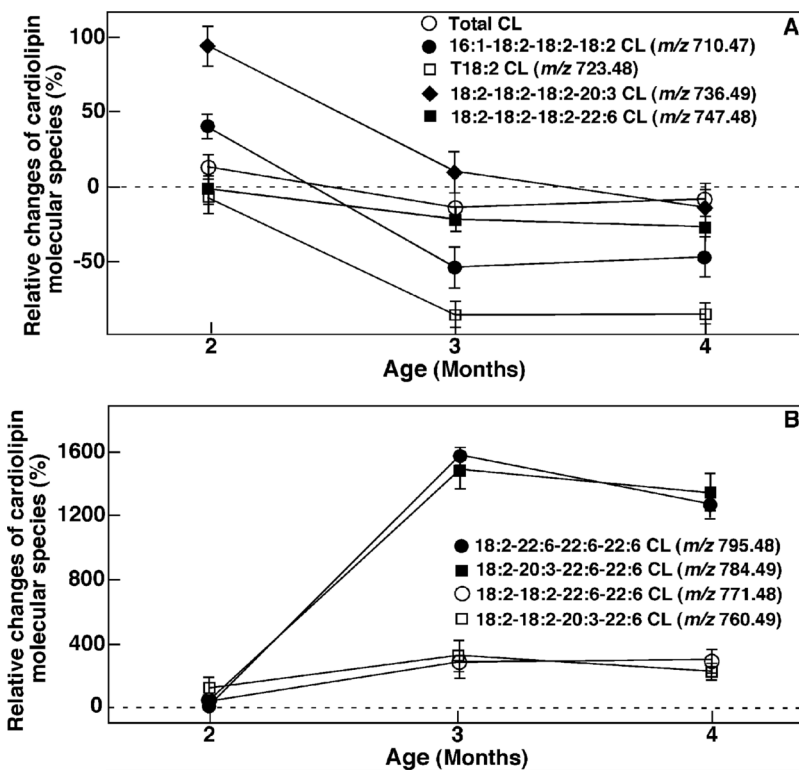
Figure 6.
Temporal changes in the quantities of selected CL molecular species in *ob/ob* mouse myocardium at different ages. Lipid extracts of mouse myocardium at different ages as indicated were performed by using a modified Bligh and Dyer method. Relative changes of individual CL molecular species as indicated were calculated in comparison to controls. Each data point represents mean ± SEM from at least four different animals.
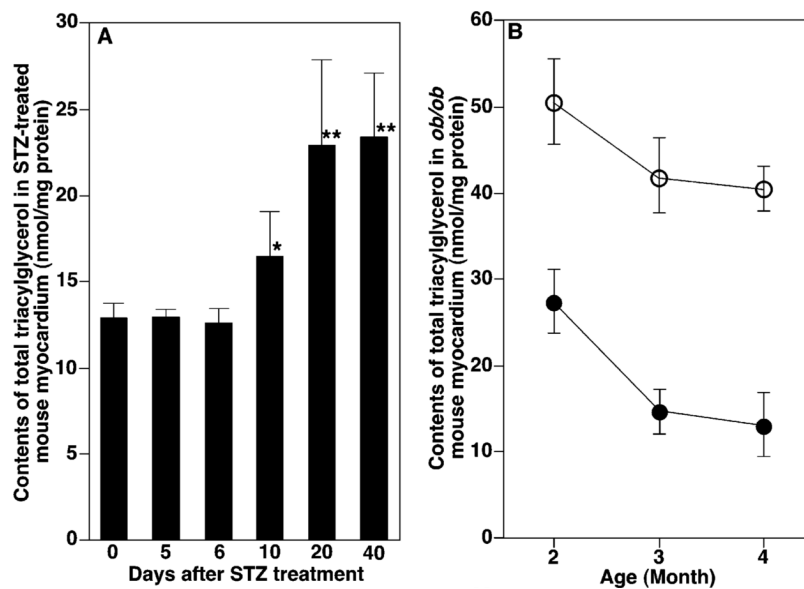
Figure 7.
Temporal course of accumulation of total triacylglycerol content in diabetic mouse myocardium. The quantities of total TG in STZ-treated mice at different time intervals after STZ injection (panel A) and *ob/ob* mice in comparison to age-matched WT mice at different ages (panel B; *ob/ob* mice, open circle; WT mice, closed circle) were determined directly from lipid extracts of mouse myocardium by using shotgun lipidomics as previously described (37). Each data point represents mean ± SEM from at least four different animals. *, $p < 0.005$ with $n = 5$. **, $p < 0.0001$ with $n = 4$.
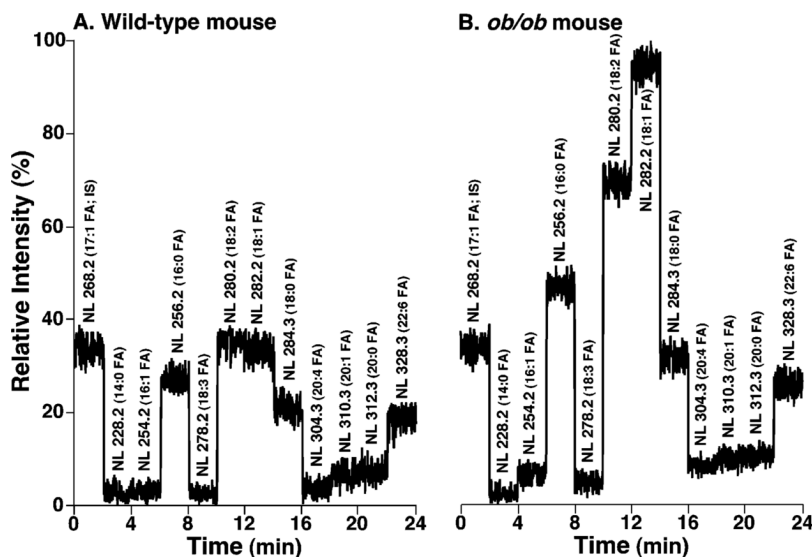
Figure 8.
Total ion current chromatogram of stepwise scanning of naturally occurring fatty acids
undergoing neutral loss from TG molecular species in myocardial lipid extracts of WT and
ob/ob mice at 2 months of age. Lipid extracts from WT (panel A) and *ob/ob* mice (panel B)
were prepared by a modified Bligh and Dyer procedure as described under Materials and
Methods and were analyzed in the positive-ion mode after infusion of the diluted lipid extracts
in the presence of a small amount of LiOH at a flow rate of 4 μL/min. In neutral loss scanning
of fatty acids, both first and third quadrupoles of a QqQ mass spectrometer were coordinately
scanned with a mass difference (i.e., neutral loss) of the selected fatty acid mass while the
second quadruple was used as a collision cell. The scan time between *m/z* 800 and *m/z* 960 was
1 s, and the total ion current of each scan was recorded for a 2 min segment. Neutral loss
scanning of all naturally occurring fatty acids was performed sequentially as indicated with 2
min for each fatty acid using a customized program operating under Xcalibur software. Due
to the facile loss of the phosphocholine headgroup, the relative contribution of fatty acyl chains
from GPCho molecular species in the mass region is small in comparison to that from TG
molecular species as previously described (37). Both TIC chromatograms were displayed after
being normalized to the TIC of NL268.2 (i.e., 17:1 FA, the internal standard for quantitation
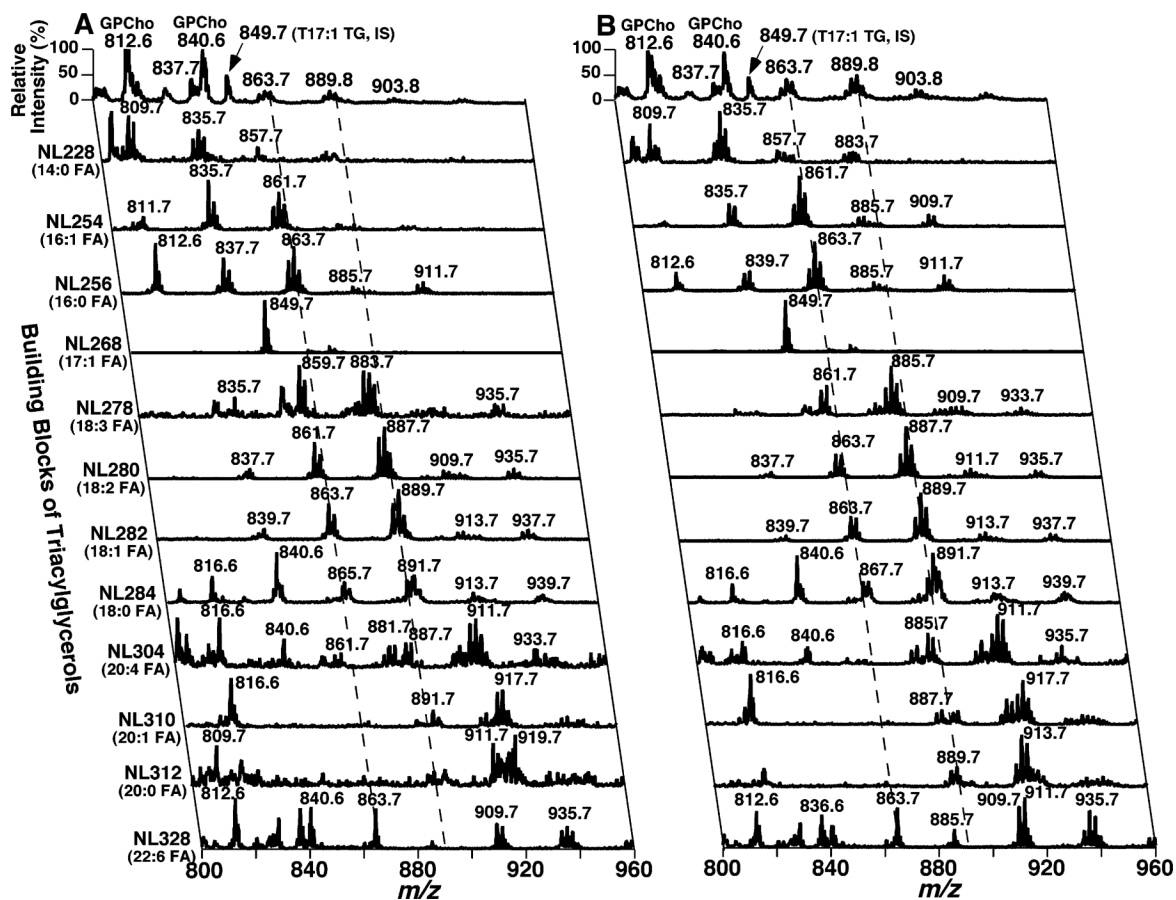of individual TG molecular species) as indicated.

Figure 9.
Two-dimensional mass spectrometric analyses of triacylglycerol molecular species profiles in myocardial lipid extracts of WT and *ob*/*ob* mice at 2 months of age. Lipid extracts from WT and *ob*/*ob* mice were prepared by a modified Bligh and Dyer procedure as described under Materials and Methods. Two-dimensional MS analyses of TG molecular species were performed in the positive-ion mode in the presence of a small amount of LiOH. Neutral loss (NL) scanning of all naturally occurring aliphatic chains (i.e., the building blocks of TG molecular species) of myocardial chloroform extracts of WT (left panel) and *ob*/*ob* mice (right panel) at 2 months of age was utilized to identify the molecular species assignments, deconvolute isobaric molecular species, and quantify TG individual molecular species by comparisons with a selected internal standard [i.e., T17:1 TG, shown in the neutral loss (NL) scanning trace of NL268.2]. Each MS/MS trace of the two-dimensional ESI mass spectra was acquired by sequentially programmed custom scans operating under Xcalibur software as shown in Figure 8. All mass spectral traces were displayed after being normalized to the base peak in each trace.
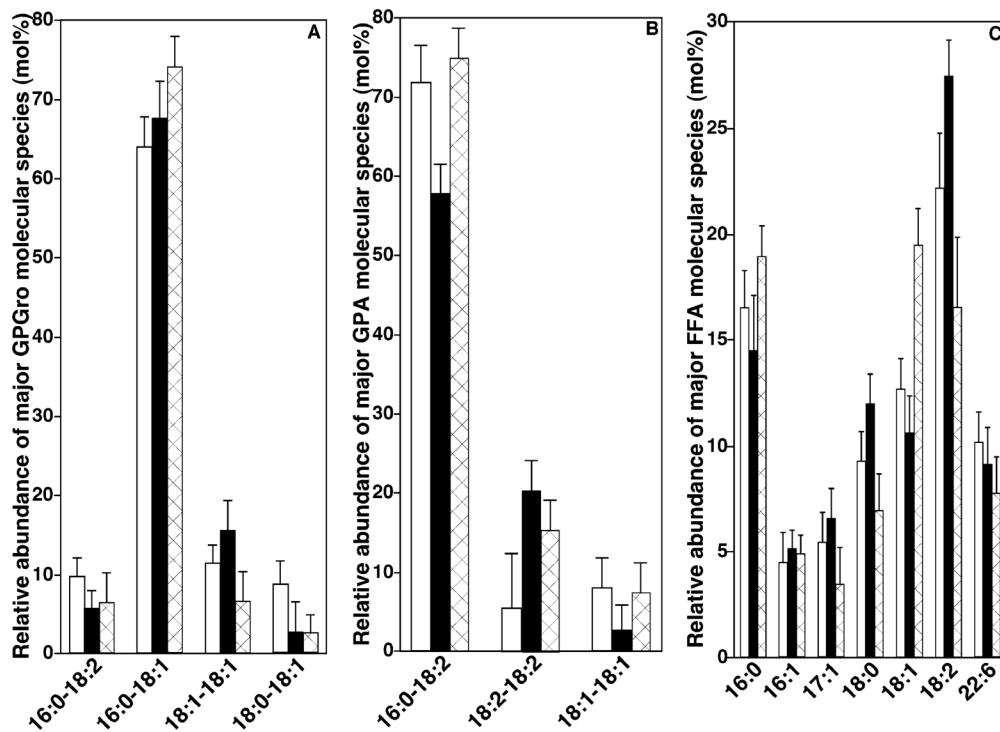
Figure 10.
Relative composition profiles of molecular species of myocardial GPA, GPGro, and FFA
classes in control and diabetic mice. Myocardial lipid extracts from control and diabetic mice
were prepared by a modified Bligh and Dyer procedure as described under Materials and
Methods. The quantities of individual molecular species of GPGro (panel A), GPA (panel B),
and FFA (panel C) in myocardial lipid extracts of control which is averaged from both control
of STZ-treated mice (4−6 months of age) and WT mice at 4 months of age (open bars), mice
for 40 days after STZ treatment (solid bars), and *ob/ob* mice at 4 months of age were determined
by shotgun lipidomics by comparison of the peak intensity of each individual ion to that of the
selected internal standards after corrections for ^{13}C isotopologue distribution differences as
described under Materials and Methods. The displayed relative composition of individual
molecular species to total content of the related class represents the mean ± SEM from at least
four different animals, and only those that are present in more than 5 mol % relative abundance
of each class are displayed.